Scattering of Radiation by Particles in Low-Altitude Plumes

R.B. Lyons,* J. Wormhoudt,† and J. Gruninger‡
Aerodyne Research, Inc., Billerica, Massachusetts

Nomenclature

A = Mie absorption efficiency
B = Planck function
C = chemiluminescence source function
f = phase function
g = first moment of phase function
N_j = line-of-sight radiance neglecting scattering
P_j = six-flux average scattering probability
Q_s = Mie scattering efficiency
S = radiation source function
s_i = ith line-of-sight segment with constant plume properties
α = aspect angle
τ_i = transmittance through the ith line-of-sight segment
σ_e = extinction optical depth
σ_s = scattering optical depth
ω = single-particle scattering albedo

Introduction

THE exhaust flowfields of solid propellant missiles may contain substantial amounts of alumina or other particles that scatter photons and, therefore, influence the radiation transport processes in such plumes. This Note studies the modification of the aspect angle dependence of the plume radiation signature, especially close to nose-on viewing when particle scattering is included.

In order to understand this effect, we will use a plume signature model that couples particle scattering to molecular and particle emission and absorption. Previous signature models, such as the Aerodyne Radiation Code (ARC),[1] treated only emission and absorption processes that need to be computed only along individual lines of sight through the plume. Scattering allows all regions of a plume to contribute to the radiation along a given line of sight, so that, in effect, the plume emission must be known before it can be calculated. A standardized infrared radiation model[2] is currently under development that will treat scattering in plumes at several levels of approximation, and solves this problem by an iterative technique leading to self-consistent emission. Our approach is to use the first iteration of a six-flux technique in ARC; that is, a model which allows a single redirection of photons through scattering. This approach is expected to be realistic if the scattering optical depth (product of scattering coefficient and path length through the plume) is small in comparison to absorption optical depth. We will use this model in an analysis of the underlying trends as scattering optical depth increases from zero.

Two calculational techniques were used to model radiation transport in missile exhaust plumes: the single scattering algorithm incorporated into the existing radiation code mentioned above, and a Monte Carlo simulation. The Monte Carlo simulation can provide as exact a solution to any specified radiative transfer problem as finite computation time will allow; in this Note, however, it has been restricted to plumes modeled as a single cylinder with uniform concentration and temperature. The ARC formulation, on the other hand, is accurate only if multiple scattering is negligible, but provides fast estimates of radiation, including particle scattering in both simple plume models and complete missile exhaust flowfields. The Monte Carlo calculations serve to test the accuracy of the single-scattering model.

We will first note the optical properties and particle size distribution appropriate to a model plume which has a 28% by weight alumina loading. We will then describe our two radiation transport models and compare the predictions of both for a uniform property (single-cylinder) plume. We will conclude by using the single-scattering model to examine the aspect angle dependence of the missile plume radiation at a visible wavelength of 0.4 μm and at an infrared wavelength of 3.74 μm.

The calculation of the optical properties of the alumina particles in the plume have been described in detail elsewhere.[3] The results are presented in Table 1, which lists the temperature-dependent refractive indices as well as absorption and scattering efficiencies averaged over the particle size distribution.

Model Plumes

This Note will consider two classes of model exhaust plumes: flowfields that are single cylinders with uniform temperature and alumina concentration, and a detailed flowfield calculated using the methods of Ref. 4 from the exit plane conditions given in Table 2. Figure 1 shows the temperature flowfield of this plume, which corresponds to an exit mass flux of 10^3 g/s, a chamber pressure of 900 psia, and a throat diameter of 1.88 cm that leads to the particle absorption and scattering efficiencies used.[3]

In the single-cylinder flowfields, emission from alumina particles alone is computed. In the detailed flowfield molecular emitters are included. At the infrared wavelength of 3.74 μm HCl contributes slightly in that the line center of the nearest HCl line is about 0.01 μm away, while at 0.4 μm CO_2 chemiluminescence due to recombination of CO and O is significant.[5]

Radiation Transfer Methods

Aerodyne Radiation Code

For single-scattering, six-flux radiation transport calculations, the exhaust flowfield is modeled by up to five concentric cylinders. Radial distributions of temperature, pressure, and species concentration at 16 axial stations in the flowfield are mapped into the selected number of cylinders by averaging over the portion of each distribution within a

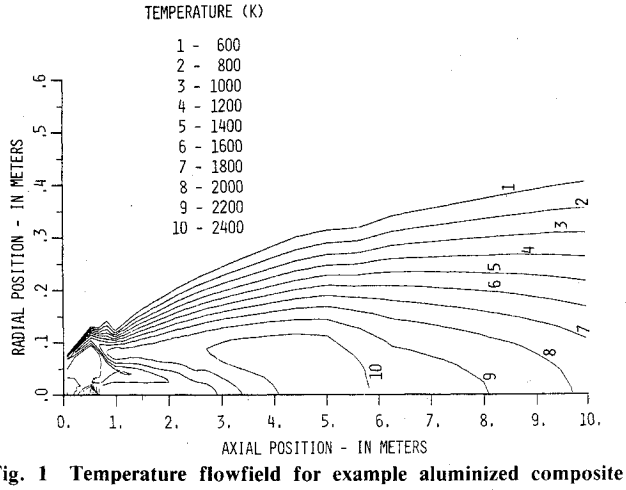

Fig. 1 Temperature flowfield for example aluminized composite propellant missile.

Received Dec. 21, 1981; revision received June 28, 1982.

*Senior Research Scientist, Center for Electro-Optical Studies. Member AIAA.

†Principal Research Scientist, Center for Chemical and Environmental Physics.

‡Principal Applied Mathematician, Center for Chemical and Environmental Physics.

Table 1 Complex refractive indices and average Mie efficiencies

	Temperature, K					
	300	1700	2000	2300	2600	2900
			Infrared, 3.74 μm			
Real refractive index	1.685	1.760	1.767	1.783	1.798	1.810
Imaginary refractive index	3.46×10^{-3}	3.46×10^{-3}	3.46×10^{-3}	3.46×10^{-3}	3.46×10^{-3}	3.46×10^{-3}
$\langle Q_A \rangle$	5.40×10^{-2}	5.60×10^{-2}	5.66×10^{-2}	5.80×10^{-2}	6.14×10^{-2}	6.34×10^{-2}
$\langle Q_S \rangle$	3.32	3.42	3.42	3.46	3.48	3.52
			Visible, 0.40 μm			
Real refractive index	1.775	1.825	1.835	1.845	1.855	1.865
Imaginary refractive index	1.00×10^{-3}	1.0×10^{-3}	3.0×10^{-3}	1.0×10^{-2}	3.0×10^{-2}	4.0×10^{-2}
$\langle Q_A \rangle$	0.136	0.123	0.354	0.844	1.33	1.42
$\langle Q_S \rangle$	3.62	3.18	2.94	2.48	2.02	1.92

Table 2 Example missile plume exit plane properties

Body radius, cm	6.4
Nozzle exit radius, cm	3.8
Exit pressure, atm	1.7
Exit temperature, K	1875
Exit velocity, m/s	2400
Major species mole fractions	
Al_2O_3	0.065
CO	0.29
CO_2	0.044
H_2	0.38
H2O	0.033
HCl	0.12
N2	0.064
Freestream pressure, atm	0.3
Freestream velocity, m/s	444

cylinder. Axial variations of the flowfield between two selected stations are modeled by up to five interpolated substations.

In order to facilitate numerical integration of the radiative transport equation, plume properties are taken to be constant within each cylindrical subdivision. The integrations are carried out along the lines of sight (LOS) that are either parallel or perpendicular to the axis of a cylinder.

The six-flux approximation to the radiative transport equation for the monochromatic radiance along an LOS s is

$$N(s) = -\frac{1}{\pi}\sum_{i=1}^{i_{\max}} S(s_i)\,(\tau_i - \tau_{i-1}) \tag{1}$$

where s_i is a plume segment along the line of sight with constant properties and τ_i is the transmittance including scattering through this segment ($\tau_0 = 1$).

The source function can be separated into two parts:

$$S(s_i) = S_1(s_i) + S_2(s_i) \tag{2}$$

where

$$S_1(s_i) = [1-\omega(s_i)]\,B(s_i) + [C(s_i)/\sigma_e(s_i)] \tag{3}$$

where $B(s_i)$ is the blackbody function, $\omega(s_i)$ is the single-particle scattering albedo, which is the ratio of optical depth due to scattering (σ_s) to total extinction optical depth (σ_e), $C(s_i)$ is the emission due to chemiluminescence, and

$$S_2(s_i) = \omega(s_i)\sum_{j=1}^{6} P_j(s_i)\,N_j^0(s_i) \tag{4}$$

where $P_j(s_i)$ is the probability that the radiation entering the j face of the six-flux box will be scattered into the s_i direction. N_j^0 is the point radiance along the line normal to the j face of the box in the absence of scattering. Physically, $S_1(s_i)$ is the source term that includes absorption, chemiluminescence, and radiation scattered out of the LOS; $S_2(s_i)$ represents radiation scattered into the LOS.

Evaluation of $S_2(s_i)$ also requires knowledge of the scattering phase function. ARC is capable of simulating both isotropic and anisotropic scattering through a suitable choice of the $P_j(s_i)$ scattering probabilities. In the isotropic case, each $P_j(s_i) = 1/6$, while for an anisotropic phase function the value of each $P_j(s_i)$ depends upon the direction of s_i. Radiation scattered into an LOS is computed with respect to a broadside-viewing grid; therefore to incorporate aspect angle dependence, the $P_j(s_i)$ used were interpolations between the broadside- and nose-on-viewing values. The two P_j perpendicular to s_i are independent of aspect angle, while, for example, for radiation propagating parallel to the plume axis away from the nozzle, the interpolated probability is

$$P_{\text{up}}(\alpha) = P_{\text{side}}(90\text{ deg})\cos^2\alpha + P_{\text{up}}(90\text{ deg})\sin^2\alpha \tag{5}$$

where α is the aspect angle (90 deg = broadside). Similar expressions hold for the other three probabilities. This form of interpolation was selected because it both conserves probability and is independent of aspect angle for isotropic scattering. Non-nose-on aspect dependence in $S(s_i)$ is calculated by extending the broadside component of LOS by $\csc\alpha$ while decreasing the axial length of the plume by $\sin\alpha$.

Monte Carlo Method

The Monte Carlo method may be used to study the propagation of photons in a medium in which both absorption and scattering take place.[6,7] As such, Monte Carlo simulation represents an alternative to (and a check on) integrations of the radiation transport equation. The Monte

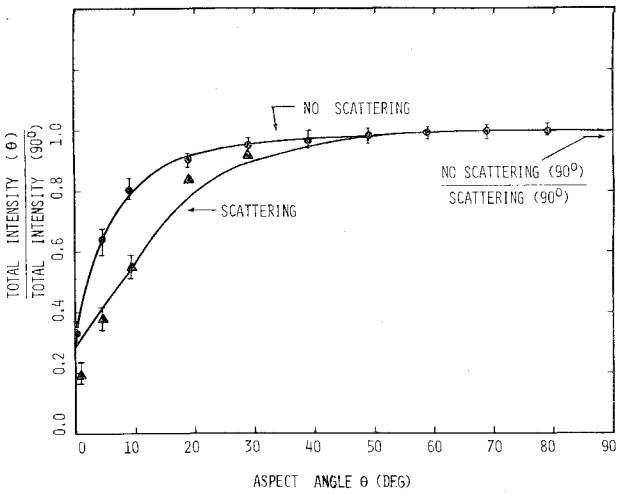

Fig. 2 Monte Carlo (▲ and ●) and ARC (solid curves) simulation of single-cylinder plume using Henyey-Greenstein phase function with $g = 0.8$. Absorption optical depth is 0.1, scattering optical depth is 0.3.

Carlo method utilizes the random selection of a physical quantity (such as the point of emission in the plume) based upon a given probability distribution. Specification of all such probability distributions defines the optical medium of interest. The plumes are assumed to be cylindrical with uniform optical properties. The inputs to the computer code were the cylinder dimensions, absorption coefficient, the scattering coefficient, and the phase function. Although these properties can be used to model any combination of radiators, the case considered here uses particle properties alone.

In modeling anisotropic scattering, the Henyey-Greenstein approximation to the phase function[8]

$$f_{HG}(\cos\theta) = \frac{(1-g^2)}{4\pi(1+g^2-2g\cos\theta)^{3/2}}$$

was used because it is easily inverted to assign a scattering angle to a particular random number. Here, g is the first moment

$$g = \int_0^{2\pi}\int_0^{\pi} f(\cos\theta)\cos\theta\sin\theta\,d\theta\,d\phi$$

of the full Mie scattering phase function $f(\cos\theta)$.

Comparison of Monte Carlo and ARC

This section presents results of Monte Carlo and ARC radiation predictions for a uniform cylinder as shown in Fig. 2. Its properties include an absorption optical depth of 0.1 across a plume diameter, a length-to-diameter ratio of 32, and in the scattering calculation, an extinction optical depth of 0.4 across a plume diameter coupled with a Henyey-Greenstein phase function with $g = 0.8$. These properties are similar to those of particles at a wavelength of 0.4 μm and a temperature of 2300 K in Table 1. At broadside viewing (an aspect angle of 90 deg), both methods predict an increase in intensity as the scattering optical depth increases from zero. This effect illustrates the redistribution of plume radiation due to scattering, which is also indicated by the fact that the aspect angle curves that include scattering lie below the nonscattering curves.

The effects of scattering on the aspect angle curves can be understood by the following argument. An optically thin plume has no aspect angle dependence (other than that due to body obscuration effects). With the addition of any source of extinction optical depth, for a model plume which is a long, thin cylinder, the intensity at off-broadside viewing decreases relative to that at broadside, due to the increased path length

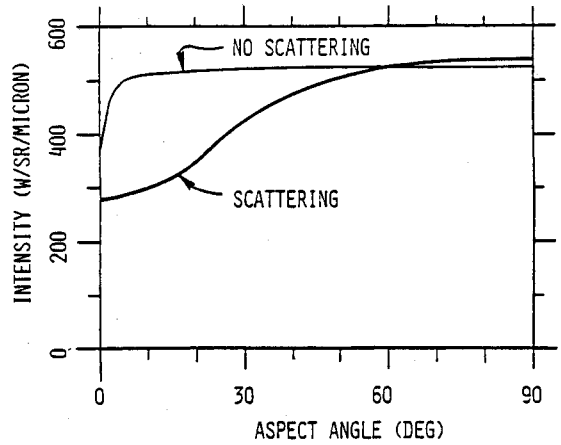

Fig. 3 ARC prediction of aspect angle dependence of model plume both with and without inclusion of scattering at a 3.74 μm wavelength.

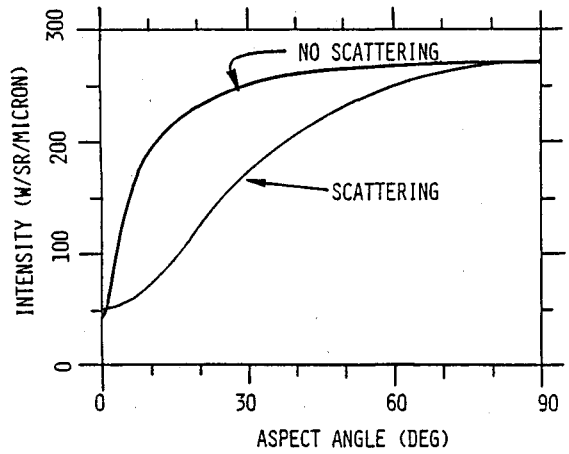

Fig. 4 ARC prediction of aspect angle dependence of model plume both with and without inclusion of scattering at a 0.4 μm wavelength.

through the plume. However, if the source of increased extinction is only increased scattering, the total intensity radiated into all angles by the plume must remain constant (see Ref. 9 for an instructive derivation). Therefore, if emitted intensities close to nose-on decrease, by conservation of emitted energy the intensities must increase in the region near broadside viewing.

The predictions presented in Fig. 2 illustrate the results of typical single-cylinder plume calculations: If the plume scattering optical depth is small enough so that little attenuation takes place in traversing a cylindrical subdivision of the ARC plume, then the six-flux, single-scattering model predictions compare favorably to Monte Carlo results for both isotropic and anisotropic scattering.

Applications to Plume Radiation

Predicted aspect angle curves for the full flowfield example plume at 3.74 and 0.4 μm are depicted in Figs. 3 and 4, respectively. The results are similar to those for the single-cylinder plumes discussed previously. For example, scattering produces a slight increase in the broadside emission at both wavelengths; however, as the aspect angle decreases from 90 deg, the predictions that include scattering decrease more rapidly than those with no scattering. At near-nose-on viewing, however, differences arise due both to the inhomogeneous temperature and species distributions and to the effects of body obscuration. In the single-cylinder plumes, the intensity at nose-on viewing is lowered when scattering is included in the calculation, because the associated increase in extinction optical depth leads to a smaller plume volume

radiating through a cylinder endcap. In the example missile plume, nonscattering predictions of aspect angle-dependent intensity depend only on the optical properties of the plume not obscured by the missile body. If scattering is included in predictions, however, then there is an additional mechanism that contributes to the nose-on intensity: The outer (colder) regions of the plume that are not obscured by the missile body can scatter radiation emitted by the inner (hotter) part of the plume that is obscured. At the visible wavelength (see Fig. 4), this extra mechanism is important, in that the 0 deg prediction that includes scattering lies slightly above that with no scattering. This may be understood by considering Table 1 and Fig. 1, which show that, in the colder regions of the plume, emission is lower and scattering is higher than in the hot portions along the plume axis. At the infrared wavelength of 3.74 μm (see Fig. 3), this additional mechanism is less important due both to the relatively small temperature dependence of emission and scattering probabilities and to the smaller volume of the emitting plume that is obscured by the missile body.

Conclusions

From the examples given in this Note we can conclude that particle scattering can indeed affect radiation predictions in both the infrared and the visible. Satisfactory quantitative results will require not only further study of calculational methods, but also further measurement of particle optical properties. In summarizing the examples presented, we note inclusion of plume scattering can lead to a slight increase in total broadside intensity. Effects become more substantial with decreasing aspect angle, in the form of lowered intensities with increasing plume path lengths. Finally, near-nose-on scattering around the body may lead to a slight increase in total intensity. This last effect, however, is, of course, very dependent on missile body size and the location of hot regions in the plume.

Acknowledgments

This work was supported in part under Contract F04611-79-C-0048 from the Air Force Rocket Propulsion Laboratory. The advice of Lawrence Bernstein, presently of Spectral Sciences, Inc., on scattering theory is gratefully acknowledged.

References

[1] Bernstein, L.S., Wormhoudt, J., and Conant, J.A., "The Aerodyne Radiation Code (ARC): Physical Assumptions and Mathematical Approximations," Aerodyne Research, Inc., Rept. ARI-RR-173, July 1979.

[2] Freeman, G.N., Ludwig, C.B., Malkmus, W., and Reed, R., "Development and Validation of Standardized Infrared Radiation Model (SIRRM) Gas/Particle Radiative Transfer Model," AFRPL-TR-79-55, Oct. 1979.

[3] Lyons, R.B., Wormhoudt, J., and Gruninger, J., "Scattering of Radiation by Particles in Low Altitude Plumes," AIAA Paper 81-1053, June 1981.

[4] Dash, S.M. and Pergament, H.S., "A Computational System for the Analysis of Mixing/Chemical/Shock Processes in Supersonic Internal and Exhaust Plume Flowfields," AIAA Paper 80-1255, June 1980.

[5] Lyons, R.B., Wormhoudt, J., and Kolb, C.E., "Calculation of Visible Radiation From Missile Plumes," AIAA Paper 81-1111, June 1981.

[6] House, L.L. and Avery, L.W., "The Monte Carlo Technique Applied to Radiative Transfer," *Journal of Quantitative Spectroscopy and Radiative Transfer,* Vol. 9, Dec. 1969, pp. 1579-1591.

[7] Meier, R.R., Lee, J.S., and Anderson, D.E., "Atmospheric Scattering of Middle UV Radiation From an Internal Source," *Applied Optics*, Vol. 17, Oct. 1978, pp. 3216-3225.

[8] Henyey, L.G. and Greenstein, J.L., "Diffuse Radiation in the Galaxy," *Astrophysical Journal*, Vol. 93, Jan.-May 1941, pp. 70-83.

[9] Viskanta, R., "Radiation Transfer and Interaction of Convection with Radiation Heat Transfer," *Advances in Heat Transfer VIII*, Academic Press, New York, 1964, pp. 175-251.